Radar Mapping Using Single Images, Stereo Pairs and Image Blocks Methods and Applications

(*) Engenheiro — Institute for National Surveying and Photogrammetry Technical University Graz, Áustria.

Abstract

The present state of mapping with radar is reviewed. Emphasis is on radargrammetric mapping with single images, stereo pairs and block adjustment. Applications to thematic mapping will be addressed as well. Examples presented conceern radar mosaicking, sea-ice study and extra-terrestrial mapping (Moon, Venus).

1. Introductions

The application of side-looking radar images to topographic mapping had been studied intensively and nearly exclusively at military agencies until a few years ago. Civilian research at that time was limited. However, while the study of military radar mapping presently seems to have been deemphasized, it is being increasingly considered for civilian tasks. A number of operational mapping projects have been carried out with radar in different regions of the world. Brasil's RADAM — project is the most daring of these. At the same time the importance of radar appears to increase as a remote sensing tool to be used in conjunction with other data. This is particulary signified by recent decisions for radar imaging from satellites.

SEASAT-A will be launched by the U.S. National Aeronautics and Space Administration (NASA) in 1978 with the main purpose of studying the ocean surfaces (waves, ice) using radar. Projects are being discussed for the SPACE SHUTTLE payload in 1980 (Operational Flight Test OFT-2) and SPACE LAB (1982 ?). Also extraterrestrial mapping is planned for Venus with a launch in 1983. In Europe similar plans exist: a radar scatterometer/side looking imager may be put into orbit with SPACE-LAB.

Simultaneously, research funds are available to take a closer look at the capabilities and limitations of radar imaging for remote sensing of sub-surface features, surface roughness, soil moisture, polarisation anomalies etc. Mapping with radar is thus a fast developing, fascinating field of study with valuable present applications and great future promise.

This short review will go over the basics of radargrammetry addressing the projection equation, stereo-radar and block-adjustment, however limiting itself to some essential facts. Then recen work will be reviewd concerning the applications of radargrammetric mapping to cartography, geology/planetology, measurement of sea-ice drift and oceanography. An attempt will be made to sketch a scenario for further progress with side-looking radar.

2. Single Image Radargrammetry

2.1 Mathematical Expressions

Radargrammetric projection equations have been formulated on many occasions in the literature. It is essential to differentiate between real-aperture and synthetic-aperture imaging. In both cases the basic fact remains that radar projection lines are circles concentric with respect to antenna (Figure 1). However, with brute force radar (real aperture) the plane of a projection cercle is normal to the longitudinal antenna axis, while with synthetic aperture radar (SAR) it is normal to the velocity vector of the antenna. From Figure 2 one may thus specify the following projection equation:

$$\mathbf{p} = \mathbf{s} + \mathbf{A}.\mathbf{r}$$

where **p**, **s** are vectors in object space, while **r** is a vector in image space, defined by unit vectors **u**, **v**, **w**. **A** is a rotation matrix.

Vector **r** is a function of slant range r, look angle Ω and a system constant Φ (squint):

$$\mathbf{r} = r\,(\sin\Phi,\ (\sin^2\Omega - \sin^2\Psi)^{1/2}\cos\Omega) \quad (2)$$

Matrix **A** describes the rotation of the image system **u**, **v**, **w** into the object system (**x**, **y**, **z**). It is defined by the classical photogrammetric ∫, ω, Ψ-angles of photogrammetry, provided however that real aperture radar is considered. For SAR it is a function of the velocity vector **s** of the antenna.

Further details may be found in the literature (Leberl, 1975; Leberl et al., 1976; Leberl, 1976). It is interesting to note that the radargrammetric difference between real-aperture and SAR has not been considerered in a majority of radargrammetric studies.

2.2 Accuracies

Single image radar mapping accuracies achieved in the past depend on a number of factors of a particular project or experiment: type of radar system, resolution, stabilisation, density of ground control, type of con-

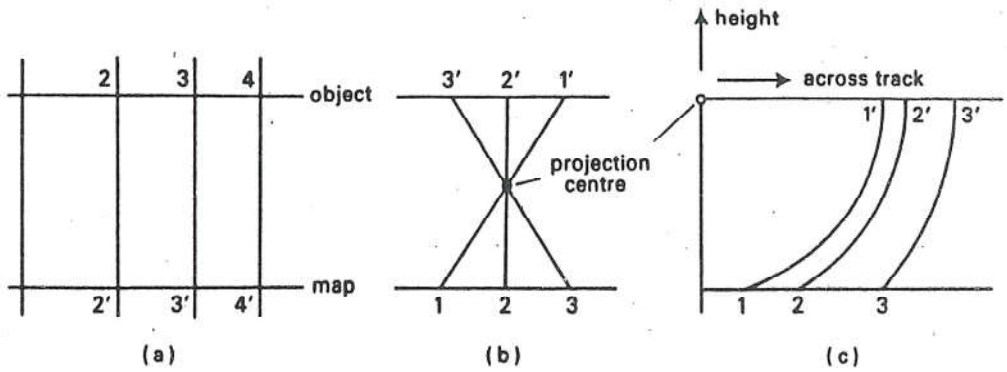

Figure 1: Projection lines for (a) the orthogonal, (b) the central and (c) the radar range projection. Note that projection lines are cercles in case (c).

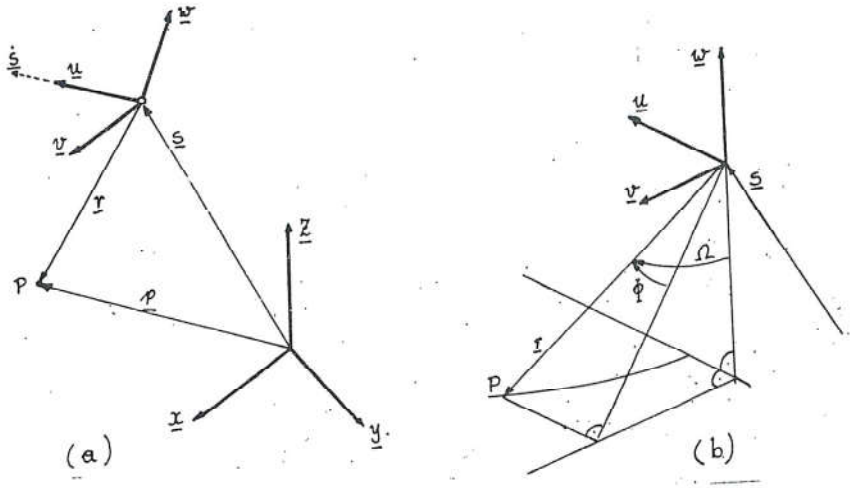

Figure 2: Definitions for the radar projection equations.

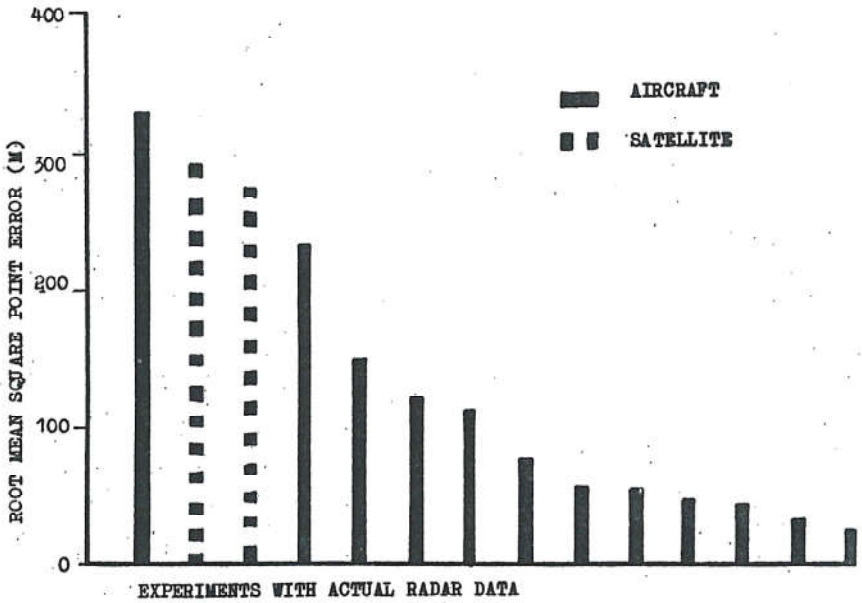

Figure 3: Accuracies achieved with single image radar mapping. Results despend strongly on specific project parameters. Satellite results are from the Apollo 17 mission to the Moon (1972).

trol, mapping method, type of terrain. Therefore results of one study may not be generalised. Figure 3 illustrates the range of results that have been obtained in the past.

In the best cases published accuracies were of the order of the ground resolution. Such results were reported e. g. by Gracie et al. (1970). Very high density of well identifiable ground control was available (about 10 points per 100 sq.km).

2.3 Rectification

Rectification is the transformation of the single radar image into a map projection. The process is usually photographical, but can also be numerical or graphical or any combination of the above. Using Equs. (1) and (2) with measured navigation data does enable one to transform a given radar image point into the map co-ordinate system (whereby the ground height must be known or assumed to be known). If in addition to navigation data also ground control points are available then the set of transformed radar image points can be matched to these control points. Generally this match may be done with some sort of interpolation algorithm. Many different procedures are possible and have been applied in the past.

While numerically the possibilities for rectification are boundless, they are limited in

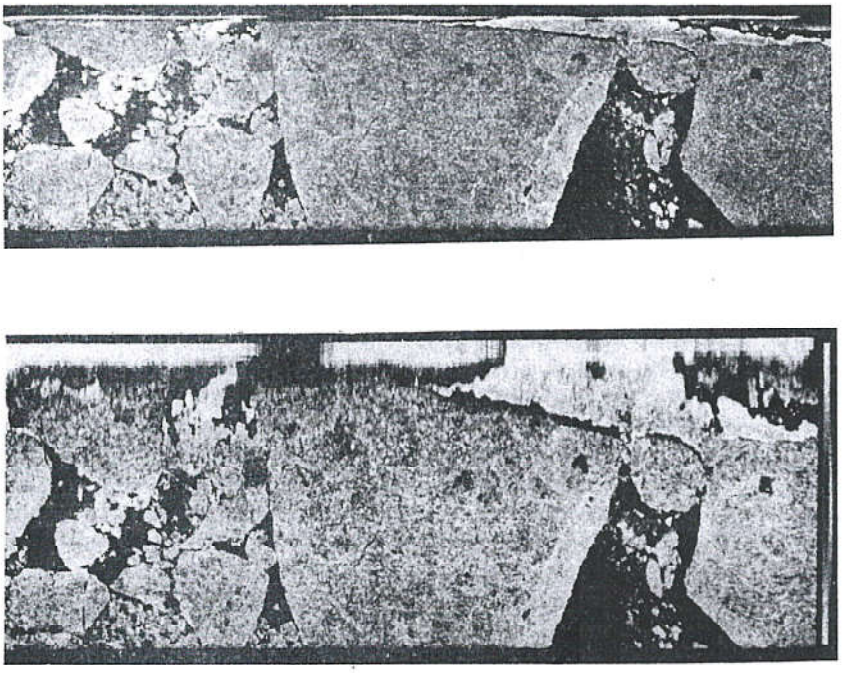

Figure 4: Example of radar image rectification using digital image processing. The distorted image (a) is in slant range presentation. Rectification is mainly a transformation to ground ranges.
(Images courtesy Jet Propulsion Laboratory, taken with L-band synthetic aperture radar system over arctic sea ice).

practice if the photographic image is to be reproduced with correct geometry. The new technology of digital image processing permits complete flexibility for rectification (see Figure 4). All geometric corrections are possible. However this rectification is very expensive and tedious indeed and therefore totally unsatisfactory for any large mapping effort.

Jensen (1974) described and optical rectifier for radar image strips to permit changes of the along-versus agross-track scales. The instrument employed anamorphic lenses. Its performance was such that the rectified images were of degraded quality. The rectification was partial only (along track scale). The solution was therefore unsatisfactory.

Peterson (1976) has extended the optical correlator (for SAR) to achieve correction of along track scale. The solution is very straightforward and does not degrade image quality. Rectification of along track scale is achieved during the conversion of signal films to map films. The simplicity of the method makes is very attractive. However, it only applies to SAR. Its implementation requires prior numerical computation to determine the amounts of image deformations. One the basis of this correction curven can be produced for the along track scale (Figure 5).

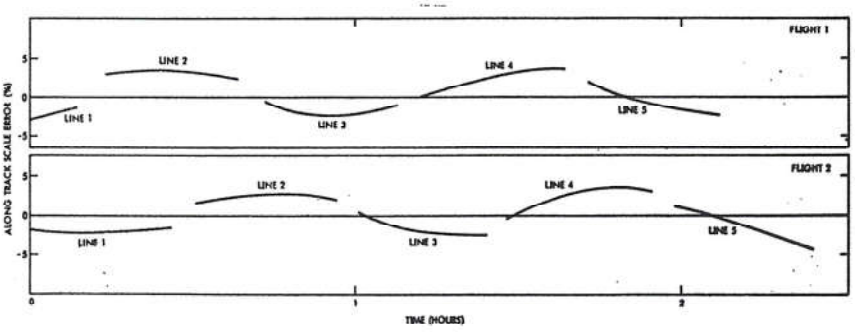

Figure 5: Scale error curves found in radar image strips (Leberl, Jensen and Kaplan, 1976). The periodicity of the along track scale errors as function of time is obvious.

3. Radar Stereo Mapping

3.1 Visual Stereo

Stereo viewing of overlapping radar imagery can greatly enhance the interpretation of the images by providing an improved means to observe morphological details, to determine slope angles and height differences and to improve cartographic mapping and point positioning accuracies.

A number of different schemes are conceitable to produce overlapping imagery in such a way that visual stereo is possible. Figure 6 illustrates the most common ones: Same side and Opposite side (LaPrade, 1963; Rosenfield, 1968). These schemes are the only ones possible for synthetic aperture radar. Cross-wise intersecting flight lines do not seem to produce valid visual stereo (Graham, 1975). Other types of stereo arrangements would be possible with real aperture radar, for example with convergent schemes using tilted antennas (Leberl, 1972; Bair & Carlson, 1974).

In order to view a three-dimensional model the two images of the stereo pair must be sufficiently similar: the image quality and object illumination must be comparable and the geometric differences (parallaxes) must not exceed a certain maximum. In photography this hardly ever presents a problem since sun angles do not change

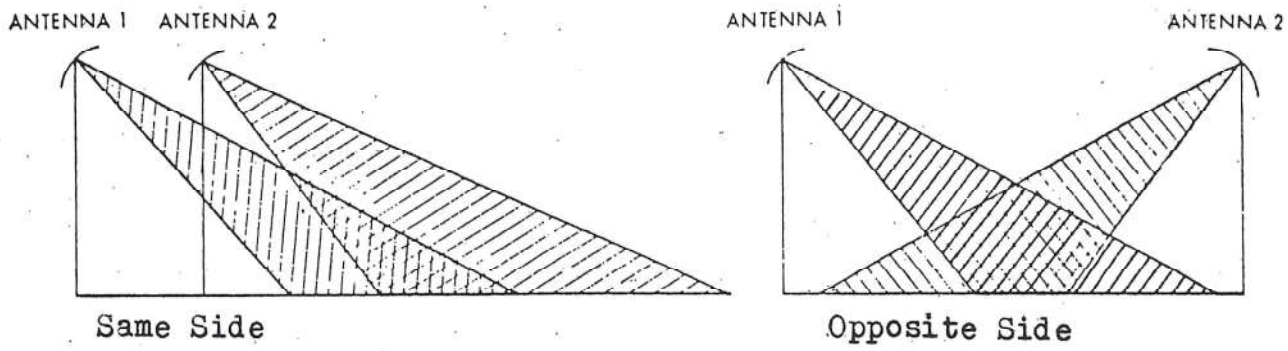

Figure 6: Basic flight configuration for stereo radar.

drastically in overlapping photos. In radar images however the illumination angles depend on the orientation and position of the sensor and so does the appearance of the images.

Figures 7 to 10 present examples of radar stereo pairs demonstrating some of the limits to stereo viewing. Figure 7 shows part of the Estrella mountains in Arizona, USA, imaged with an opposite side arrangement from an aircraft at 12 km altitude. It can be seen that slopes that reflect strongly in one image are in the radar shadow in the other image. A stereo impression can be obtained in the flat areas of this stereo pair, but becomes very difficult in the mountains. Figure 8 demonstrates with a same side stereo pair taken with the same radar system, that there are no problems to stereo viewing.

Figures 9 and 10 present two Apollo 17 satellite radar stereo pairs taken of the lunar surface with same side geometry and very small stereo base. Look-angles however are much steeper than in the examples of Figure 7 and 8. This leads to larger relief displacements and to differences of image contents in the stereo-mates even with small stereo bases. In the flat part of Figure 9 stereo viewing is not difficult. However, in the Apennin mountains stereo fusion becomes nearly impossible. This is even more so in Figure 10 taken over the rugged Oriental region on the Moon's for side.

Figure 7: Example of same side stereo radar model of Estrella Mountains in Arizona, USA.

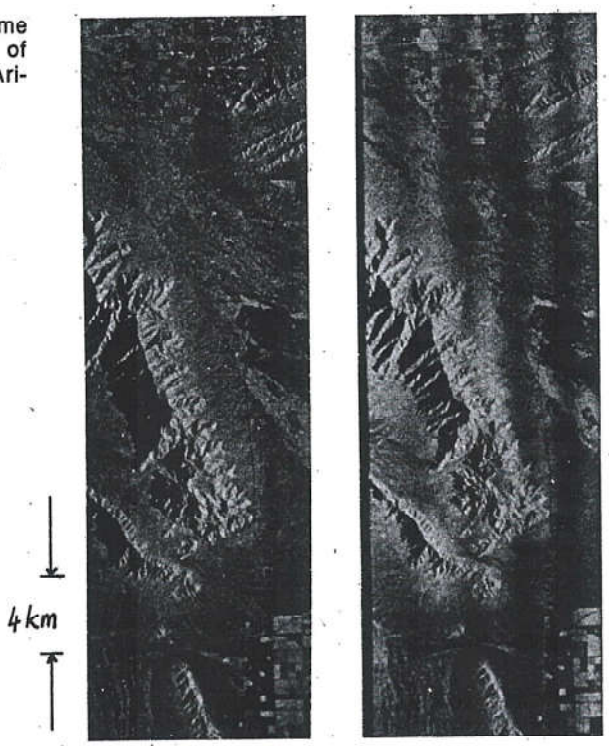

From the above examples the following factors influencing radar stereo viewing can be identified:

Stereo arrangement (same-side, opposite side);
Look angles (angles off-nadir);
Stereo intersection angles;
Ruggedness of the terrain.

Exact interrelations among these factors are presently not well understood. Past experiences lead however to the tentative conclusion that opposite side stereo can only be applied in cases of flat or rolling surfaces, while rugged terrain requires same side imaging. Stereo viewing improves with shallower look angles (45° off-nadir and more). With steeper look-angles (near nadir) the stereo base has to reduce for successful stereo viewing, thereby leading to reduced accuracy.

3.2. Stereo Computation

Proper radar stereo computations may stard off from Equs.

Figure 8: Example of opposite side stereo radar model, area same as in Figure 7.

Figure 9: Example of lunar satellite radar stereo model of the Apennin mountains. Stereo base is very small (3° angles of intersection). Good stereo viewability. (Courtesy Jet Propulsion Lab.).

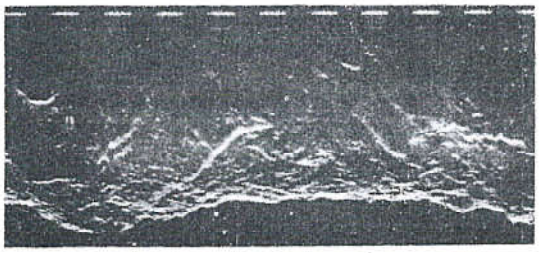

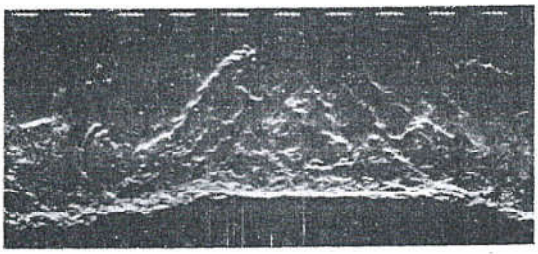

Figure 10: Lunar radar stereo model of the Oriental region on the Far Side of the Moon. Stereo viewability is poor. Same side geometry. (Courtesy Jet Propulsion Laboratory, USA).

(1) and (2) where vector **p** is the unknown and to be found from:

$$\mathbf{p} = \mathbf{s}' + \mathbf{A}'\,\mathbf{r}'$$
$$\mathbf{p} = \mathbf{s}'' + \mathbf{A}''\,\mathbf{r}''$$

where (') denotes the left and (") the right image.

A simplified formulation is obtained when one assumes a stereo pair with parallel, perfectly straight and level flight lines. Figure 11 shows that in a ground range presentation a stereo parallax Δp can be found that relates to ΔH as follows:

$$\Delta H = p'/\tan\Omega'$$
$$\Delta H = p'' / \tan\Omega''$$
$$\Delta p = p' - p'' = \Delta H\,(\tan\Omega' - \tan\Omega'')$$
$$\Delta H = \Delta p / (\tan\Omega' - \tan\Omega'')$$

Equ. (4) is valid only if the projection cercles can be approximated by straight lines p_a, p_b (Figure 11).

The situation for slant range geometry is slightly more complex. Even a flat ground will appear to be bowed in the radar stereo model. A discussion of this can be found in Leberl (1977) or in Leberl and Elachi (1977).

3.3 Accuracies

The range of accuracies achieved so far with stereo radar is similarly wide as that of single image mapping. Also here a large series of factors is of influence.

Figure 12 illustrates height accuracies obtained in the past. A conclusion may be that accuracies range from the resolution up to many tens of times the resolution, whereby stereo-arrangement and control density are the main factors of influence. A study by Gracie et al. (1970) concluded that stereo height measurements would be accurate to within ± 13 m. However the result applies to a density of 35 control points per 100 sqkm and very well identifiable test Dewideit (1977) achieved a + 25 m root mean square height error

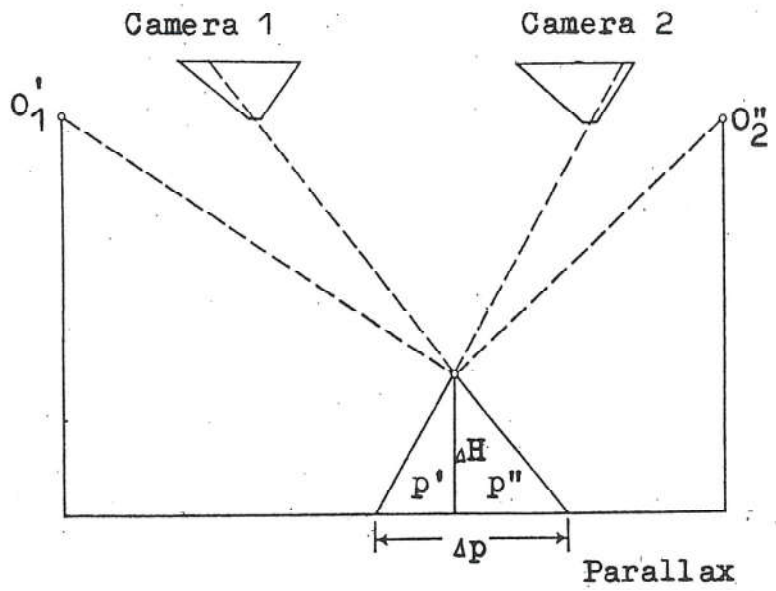

Figure 11: Definitions for the simple stereo computation with side-looking radar. The stereo base 01 02 of radar corresponds to a camera stereo base of (Camera 1 to Camera 2) to produce equivalent parallaxes.

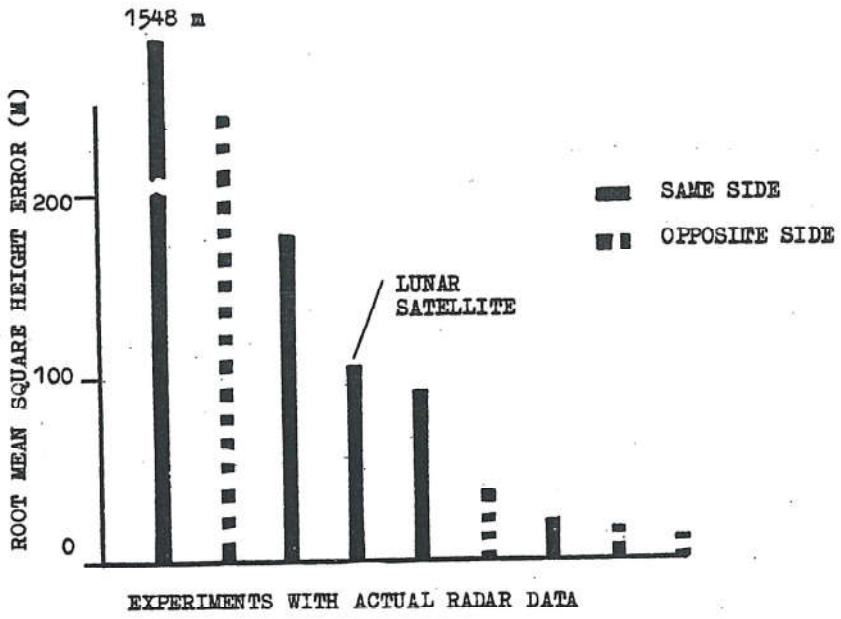

Figure 12: Accuracies achieved in experiments with radar stereo. Results strongly depend on project parameters.

root mean square height error using triple overlaps and high density of control. The computing effort was very considerable. With a more modest (and realistic) density of control that corresponds to a reconnaissance type survey, say 4 points per 10 000 sq km, height accuracies may deteriorate to ± 100 to ± 200 m and more (see for example Derenyi, 1975; Leberl, 1977 a).

The future may bring about an improved radar stereo capability from aircraft sensors only if navigation improves; and from satellite sensors only if look angles are varied sufficiently from one pass to the overlapping one over a given area. However, the active mode of operation causes an inherent weakness of stereo: differing image contents if look angles vary, good visual stereo fusion only with very similar look angles.

4. Block Adjustment and Mosaicking

4.1 General

Actual radar mapping projects result in blocks of overlapping image strips (Radam: 25%, Proradam: 60%, West-Virginia: 25% and 60%). Mapping should thus be based on an adjustment to densify the generally sparse net of control points and to take advantage of the available redundancy in the overlaps. So far radar block adjustment has been applied to planimetry, using the original images (Leberl, 1975; Leberl, Jensen and Kaplan, 1976). Threedimensional radar block adjustment has been studied in a laboratory environment by DBA-Systems (1974) and by Dowideit (1977). The approaches however were not practical under present constraints.

Radar mosaicking has been carried out on three levels of sophistication: (a) no control points are used. The images are simply compiled to fit each other into mosaics; (b) production strips are flown along parallel lines (for example north-south) and tie-lines are flown across (for example east-west). The tielines are controlled by ground control points or by tracking of the aircraft (e.g. Shoran) and the production lines are compiled into mosaics to fit the tie-lines; (c) all production strips are controlled by continuous tracking of the aircraft (Shoran); or a block

adjustment is carried out to control all radar images for mosaicking.

Of these the most satisfactohave been mapped notonly in South America, but also in Africa and other parts of the world.

A recent extension of the mere use of radar for mapping is the image strips (Peterson, 1976) in a recorrelation. Mosaicking is greatly simplified by the method as compared to other approaches.

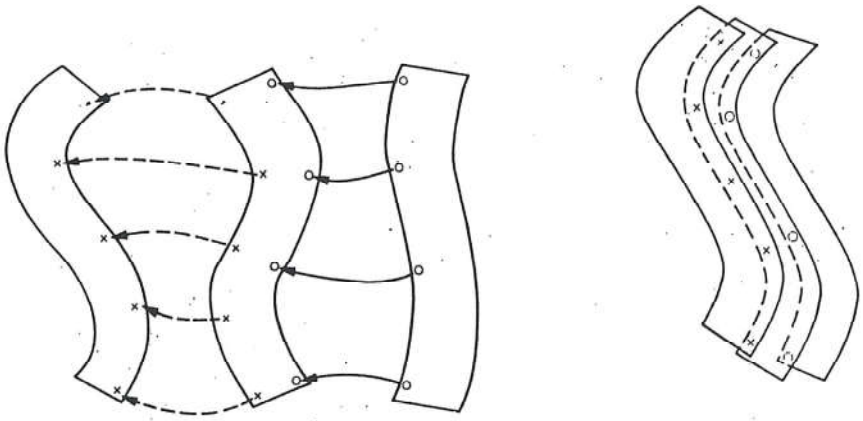

Figure 13: Principle of internal radar block adjustment. Tie-points are used to tie the strips (or stereo models) into a coherent block.

4.2 Method of Block Adjustment

Internal Adjustment

The block adjustment is based on a fit of the radar image strips with respect to each other overlap of images (Figure 13). A coherent image block is a obtained as shown in Figure 13 (b). Spline functions are used to describe image corrections $_{\Delta}x$ (along flight) and $_{\Delta}y$ (across flight). A spline consists of pieces of polynomials according to Figure 14; each of the pieces is:

$$_{\Delta}x = a_{io} + a_{i1}\,(x - x_i) + a_{i2}\,(x - x_i)^2 + a_{i3}\,(x - x_i)^3 \quad (4)$$

$$_{\Delta}y = b_{io} + b_{i1}\,(x - x_i) + b_{i2}\,(x - x_i)^2 \times b_{i3}\,(x - x_i)^3$$

where the condition applies:

$$x_{i-1} \leqslant x < x_i \quad (5)$$

This condition amplies that a polynomial piece is valid only in the range delimited by values x_{i-1} and x_i.

Additional conditions apply to enforce a smooth transition from one polynomial piece to the next: the derivatives of Oth, 1st, 2nd order are made identical at the joints of polynoms. We find:
for the function value (Oth derivative):

$$a_{io} \pm a_{i1}.D + a_{i2}D^2 + a_{i3}.D^3 = a_{i+1,o} \quad (6)$$

for the tangent (1st derivative):

$$a_{i1} + 2a_{i2}.D + a_{i3}.D^2 = a_{i+1,1} \quad (6)$$

for the curvature (2nd derivative):

$$2a_{i2} + 6a_{i3}.D = 2a_{i+1,1} \quad (8)$$

D is the length of the polynominal piece:

$$D = x_{i+1} - x_i \quad (10)$$

External Adjustment:

The coherent radar image block must be transformed into the net of ground control points. The principle is illustrated by Figure 15. Any method of interpolation can be used to fit the image block to the control points.

Internal and external adjustment can be carried out sequentially or simultaneously. A sequential solution has the advantage of low programming and computational efforts. The ge-

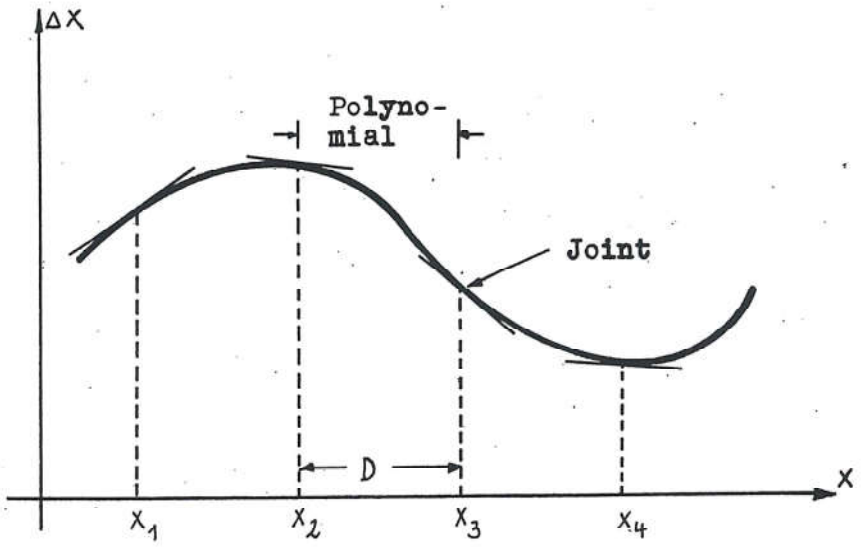

Figure 14: Spline-function or piece-wise polynomial. The function is composed of polynomial pieces defined over a range D. Conditions exist at joints that adjacent polynomials are not discontinuous.

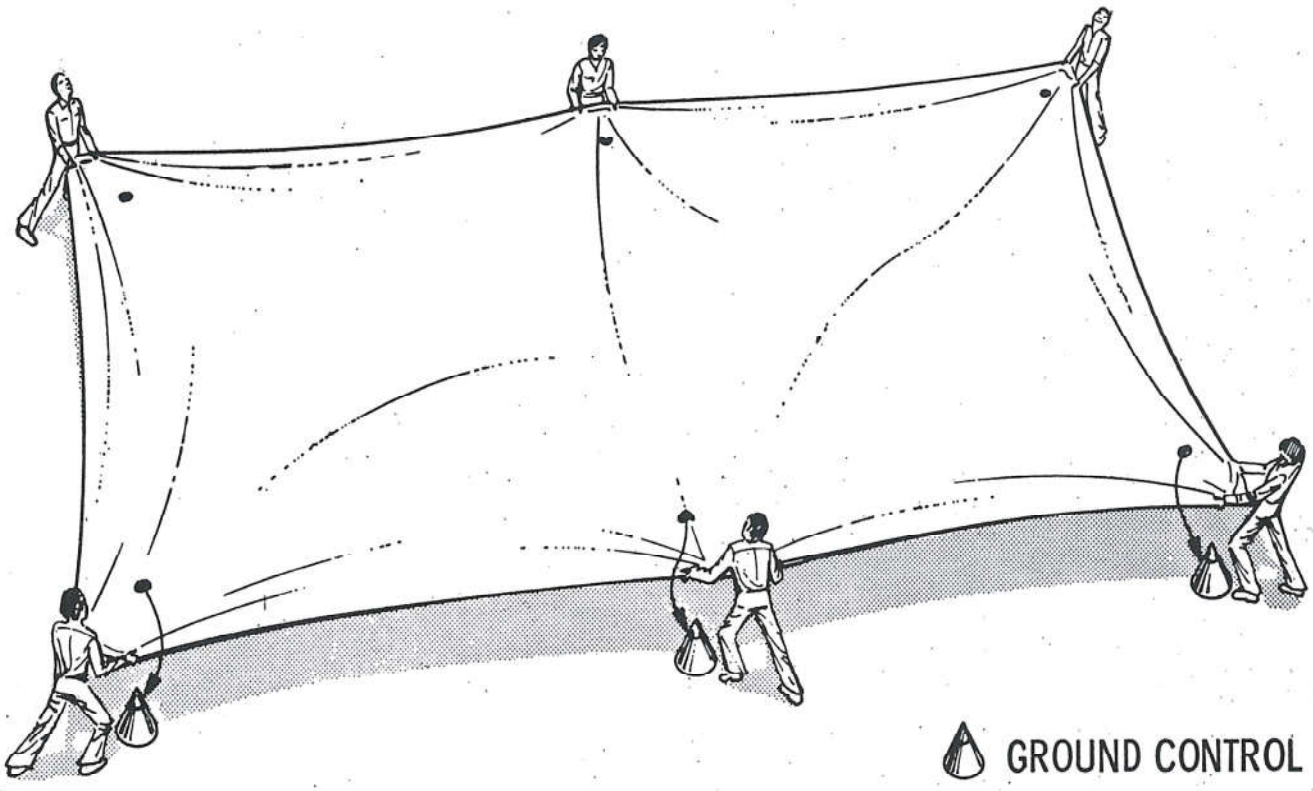

Figure 15: Principle of external radar block adjustment: the coherent block is made to fit to the ground control points.
Methods of fitting are numerical interpolation.

nerally limited density of ground control and dominating effect of periodical ("systematic") image errors permit to conclude that a sequential solution does not produce results significantly inferior to a simultaneous approach (Leberl, 1974).

4.3 Results

Block adjustment accuracy has been evaluated in a controlled experiment with images from the U.S.A. (Leberl, Jensen, Kaplan, 1976). The result is shown in Figure 16. The abszissa shows the density of control, the ordinate the root mean square point errors in check points. The images had sidelaps of 20%.

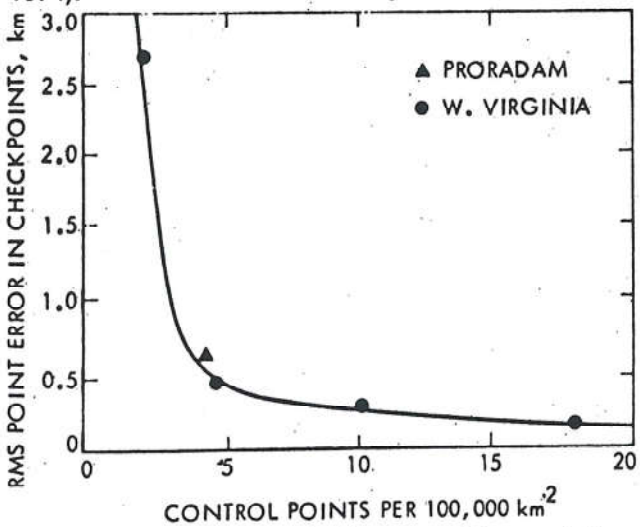

Figure 16: Accuracy of radar block adjustment for mosaicking: data are from an experimental radar block in West-Virginia (Leberl, Jensen and Kaplan, 1976) and from the Colombian Proradam (Leberl, 1977a).

An equal distribution of ground control produces the best results. A point density of 15 points per 100 000 sqkm can result in r.m.s. point errors of about ± 150 m (or coordinate errors of ± 100 m).

DBA-Systems (1974) and Dowideit (1977) obtained results that were about 3 x the resolution of the radar images, however using an unpractically high density of about 10 control points per 100 sq km (1000 points per 100 000 sq km!).

5. Some Recent Applications of Radar Mapping

5.1 Geology / Planetoly

The application of side-looking radar for mapping the geo-

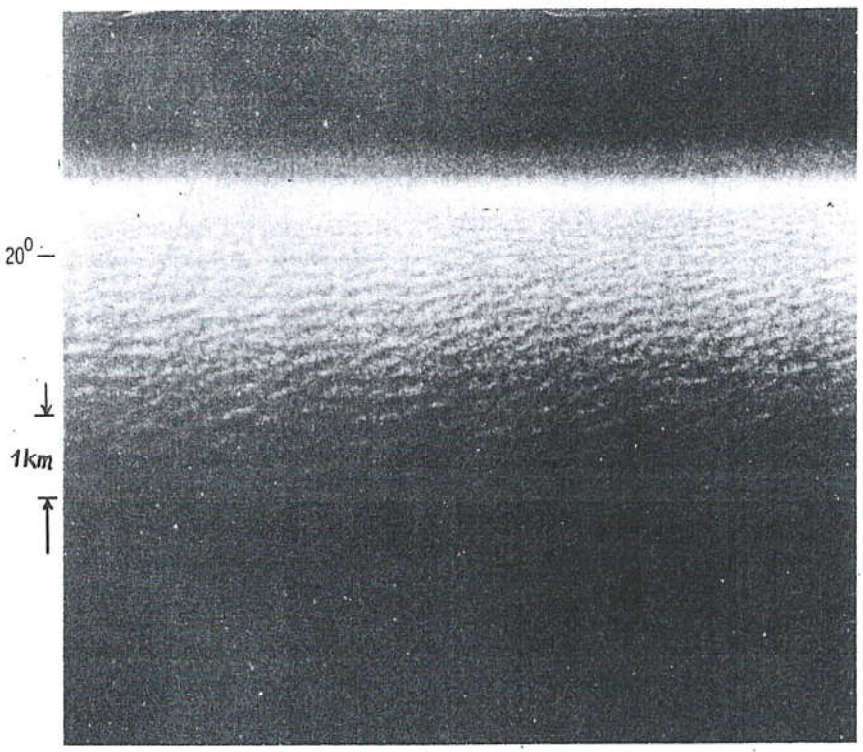

Figure 17: Example of a radar image of ocean waves taken with the L-band SAR of the Jet Propulsion Laboratory, USA.

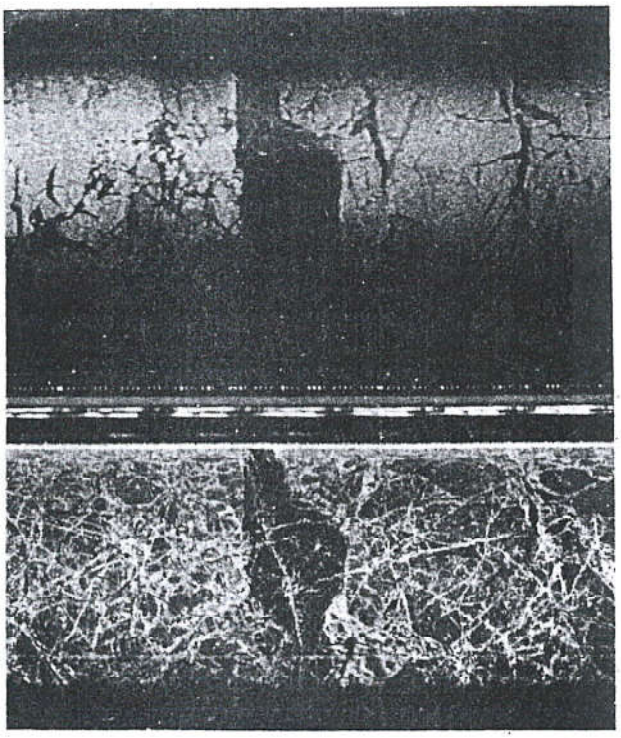

Figure 18: Examples of SAR images of arctic sea ice at wavelengths of 3 cm (above) and of 25 cm (below) (× — and L-band). (Courtesy of Jet Propulsion Laboratory, USA).

logy or surface of the Earth and of other planets (Moon, Venus) is based on two kinds of information:

(a) they show topographic detail, vegetation borders, drainage etc and are thus used like photography;

(b) radar image brightness is related to surface roughness and dielectric constant. It is thus an indicator for soil moisture in vegetated areas; and for surface roughness in arid areas.

Particularly the item (b) is one of great promise for the future role of SAR and SLAR. Work is under way to fully understand this phenomenon. A number of satellite projects are planned to evaluate the use of radar for geologic mapping (Shuttle OFT-2 in 1980; Space-Lab in 1982). A planetary mision to Venus is planned for 1983 (Venus Orbital Imaging Radar — VOIR) to explore the planet's surface topography and geology.

5.2 Oceanography

An important satellite side-looking radar experiment is SEASAT-A with a launch planned for May 1978. Radar images are to be producet of the ocean surface to study wave pattern (Figure 17) and related ocean surface phenomena.

5.3 Sea and Lake Ice

Figure 18 presents two examples of arctic sea ice images produced with and aircraft SAR at wavelengths λ = 3 cm and λ = 25 cm (X-and L-band). Sea- and lake-ice can very well be imaged and studied with radar images. The longer wavelength radar penetrates through the snow cover and through part of the ice. The image appears therefore different from the shorter X-band radar wavelength. Ice images permit the study of ice motion (Leberl et al. 1976) and enable the shipping routes to be constantly monitored, even under adverse weather and ice

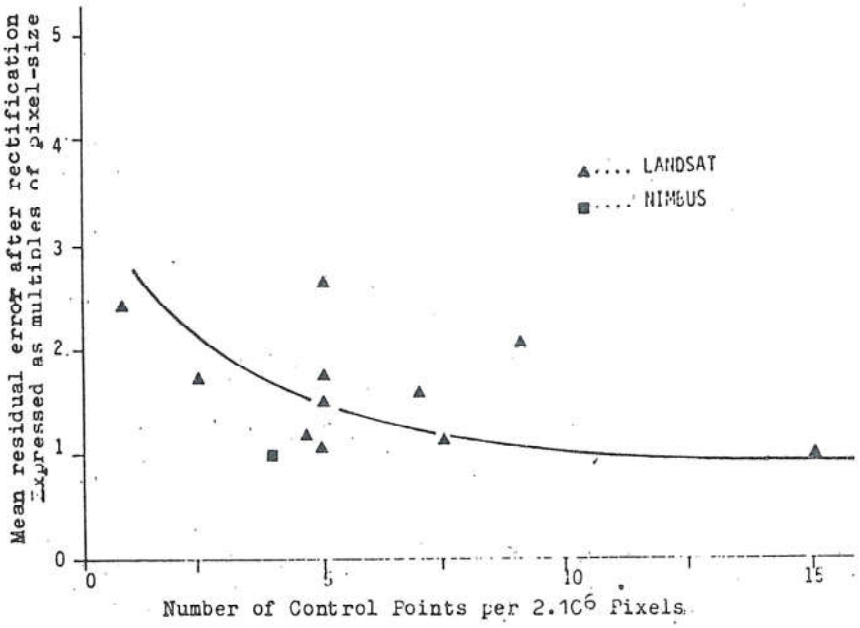

Figure 19: Accuracy of planimetric mapping with satellite scanner images, expressed in multiples of the pixel size (Pixel size of Landsat is about 80 m, for Nimbus about 9.5 km).

conditions (Schertler et al., 1975).

5.4 Cartographic and Thematic Mapping

From the above it is evident that side looking radar can also be used for cartographic mapping reconnaissance surveys for land use, forestry, soils etc. Brasil's Radam (Roessel and de Godoy, 1974) was and is a prime example for this. Large regions have been mapped not in South America, but also in Africa and other parts of the world.

A recent extension of the mere use of radar for mapping is the combination was only experimental and purely for the purpose of enhanced image interpretation. The geometric accuracy of satellite imaging with Landsat scanner data is however such that the combined use of satellite images and tation. The geometric accuracy of satellite imaging with Landsat scanner data is however such that the combined use of satellite images and radar radar should also be considered for cartographic (geometric) mapping. Figure 19 presents experimental results of geometric mapping with Landsat (Leberl, 1977). It turns out that a relatively modest control density can already lead to mapping accuracies of about ± 70 to ± 100 m (coordinate errors).

A next step of cartographic radar mapping would thus be the combined block adjustment with satellite and airborne scanner and radar images.

6. Conclusion

Radar earth science applications otherthan the classical ones to general purpose land mapping and delineation of geological lineamants are rapidly being developed. Major recent applications concern planetology, surface roughness, soil moisture, ocean waves, sea-and lake ice, vegetation types and health, snow surveys etc. Several satellite projects promise to help furthel development of radar applications (Seasat A, Space Shuttle OFT-2, Space-Lab, VOIR).

The applications rely in part on radargrammetric processing of the image strips. Basic facts are here reviewed concerning single images, stereo and block adjustment. It is shown that radar block adjustment on a digital computer, even with modest effort can produce co-ordinate accuracies of about ± 100 m.

References

Bair L.G. and G.E. Carlson (1975) Height Measurement with Stereo Radar, **Photogrammetric Enginnering and Remote Sensing**, Vol. XLI.

DBA-Systems (1974) **Research Studies and Investigations for Radar Control Extensions**, DBA-Systems Inc., P.O. Drawer 550 Melbourne, Florida, USA, Defense Documentation Center Report No. 530784L.

Derenyi E.E. (1975) Topographic Accuracy of Side Looking Radar Imagery Paper presented at the 41 st Angrammetry (ISP), 13th Congress, Society of Photogrammetry, Washington D.C.

Dowideit G. (1977) Eine Blockausgleichung für Aufzeichnungen des Seitwarts-Radar (SLAR), **Bildmessung und Luftbildwesen**, Nr. 1, Volume 45 pp. 17-23.

Gracie G. et al. (1970) **Stereo Radar Analysis**, USAETL, Ft. Belvoir, Virginia, Report No. FTR-1339-1.

Graham L. (1975) Flight Planning for Stereo Radar Mapping, **Photogrammetric Engineering and Remote Sensing**, Vol. XLI.

Harris G. and L. Graham (1976): Landsat Radar Synergism, Presented Paper, International Society for Photogrammetry (ISP), 13th Congress, Helsinki, Finland.

Jensen H. (1974) Deformations of SLAR Imagery — Results from Actual Surveys, Proceedings, Symposium of Comm. III of ISP, Stuttgart, F.R.G., in Deutsche Geodatische Kommission, Series A, Nr. 214.

LaPrade G. (1963) An Analytical and Experimental Study of Stereo for

Radar, **Photogrammetric Engineering**, Vol. XXIX.

Leberl F. (1975) Sequential and Simultaneous SLAR Block Adjustment, **Photogrammetria**, Vol. 31, No. 1.

Leberl F., H. Jensen, J. Kaplan (1976) Side-Looking Radar Mosaicking Exriment, **Photogrammetric Engineering and Remote Sensing**. Vol. XLII.

Leberl F., T. Farr, L. Bryan, C. Elachi (1976) Study of Arctic Sea Ice Drift from L-Band Side Looking Radar Imagery, **Proceedings**, 42nd Annual Convention of the American Soc. for Photogrammetry, Washington D.C., USA.

Leberl F., C. Elachi (1977) Mapping With Satelite Side-Looking Radar, **Proceedings**, GDTA Symposium on Remote Sensing, Paris, France, September, 21 — 23.

Leberl F. (1977 a) Imaging Radar Applications to Mapping and Charting **Photogrammetria**, Vol. 32.

Leberl F. (1977 b) Herstellung von Kartenunterlagen mittels Satellitenphotographie und Fernerkundungsverfahren, **Geowissenschaftliche Mitteilungen**, Technische Univ. Vienna (in press).

Peterson R.K. (1976) The Correction of Anamorphic Scale Errors in Holographic Radar Imagery, Goodyear Aerospace Scale Errors in Holographic Radar Imagery, Goodyear Aerospace Corp. Report Code 99696, Litchfield Park, Arizona, USA

Roessel J. van, R. de Godoy (1974) SLAR Mosaics for Project RADAM, **Photogrammetric Engineering**, Vol. XL.

Rosenfield G.H. (1968) Stereo Radar Fechniques, **Photogrammetric Engineering**, Vol. XXXIV.

Schertler R.J. et al. (1975) Great Lakes All-Weather Ice Information System, **Proceedings**, 10th Symposium on Remote Sening of the Environment, Ann Arbor, Michigan, USA.

SÓCIO DA SBC NA CHEFIA DE CURSO NA EsIE

Depois de ocupar a subchefia da 2ª Divisão de Levantamento do Serviço Geográfico do Exército, e de breve passagem, de retorno, ao COC, assume a Chefia do Curso de Formação de Sargentos Topógrafos da EsIE, o nosso muito caro sócio e amigo TC Norival dos Santos Júnior. É para a SBC motivo de muita satisfação este evento pois se constitui em argumento forte para que fortaleçam nossas relações de amizade junto àquele conceituado centro de instrução especializada.

IBGE recomenda adoção do Datum SAD-69

Como se sabe o IBGE é o Órgão Nacional responsável pelo estabelecimento da Rede Geodésica de Apoio Fundamental no território brasileiro.

Em conseqüência dessa responsabilidade, é ainda, o Órgão que dita as normas para esse tipo de trabalhos e, também, determina o melhor ponto de referência para ajustamento das cadeias de triangulação e da malha de poligonais, ou seja o "Datum".

Dentro dessa ordem de idéias e,

— considerando terem sido concluídos os estudos gravimétricos e astrogeodésicos definitivos para o estabelecimento do Datum Brasileiro;
— considerando que esse Datum está sendo adotado por todos os países do Continente Sulamericano e, em conseqüência será o Datum Sulamericano, cuja sigla é DSA, mais conhecido como SAD-69;
— considerando que o Datum Astronômico de Córrego-Alegre, até então utilizado como ponto de referência para o mapeamento sistemático, é provisório;
— considerando que a diferença entre um e outro é pouco significativa no campo cartográfico;
— considerando que o Datum de Córrego-Alegre já não satisfaz à finalidade geodésica se se considera a extensão do Continente Sulamericano;
— considerando que deve haver uniformidade de princípios, quer se trate da finalidade geodésica ou cartográfica.

Conclui o IBGE:

Que se utilizem, para todas as finalidades, os novos valores do Datum SAD-69, cuja origem é o Vértice de Triangulação Chuá, situado nas proximidades da cidade de Uberaba-MG, de Coordenadas Geodésicas, Azimute para o vértice Uberaba (a partir do Sul) e Afastamento Geoidal, seguintes:

Latitude -19° 45' 41.6527"S
Longitude 48° 06' 04.0639"W
Azimute 271° 30' 04.05"
Afastamento Geoidal N = 0 m.

Os parâmetros do elipsóide de referência são:

Semi-eixo maior
a = 6 378 160 m.
Achatamento f = 1/298.25